

Magnetic Resonant X-Ray Scattering in KCuF_3

Manabu Takahashi

Faculty of Engineering, Gunma University, Kiryu, Gunma 376-8515, Japan

Manabu Usuda and Jun-ichi Igarashi

Synchrotron Radiation Research Center,
Japan Atomic Energy Research Institute,
Mikazuki, Sayo, Hyogo 679-5148, Japan

(Dated: October 31, 2018)

We study the magnetic resonant x-ray scattering (RXS) spectra around the K edge of Cu in KCuF_3 on the basis of an *ab initio* calculation. We use the full-potential linearized augmented plane wave method in the LDA+ U scheme, and introduce the lattice distortion as inputs of the calculation. We obtain finite intensity on magnetic superlattice spots, about three orders of magnitude smaller than on orbital superlattice spots, by taking account of the spin-orbit interaction (SOI). No intensity appears without the SOI, indicating that the intensity arises not from the spin polarization but from the orbital polarization in $4p$ states. The present calculation reproduces well the experimental spectra as functions of photon energy and of azimuthal angle. We also calculate the RXS intensity on orbital superlattice spots. It is found that the intensity increases with increasing Jahn-Teller distortion. The spectra remain nearly the same in the nonmagnetic state given by the simple LDA, in which the orbital polarization in the $3d$ states is much smaller. This strongly suggests that the intensity on orbital spots is mainly controlled by the lattice distortion, not by the $3d$ orbital order itself.

I. INTRODUCTION

The resonant x-ray scattering (RXS) has attracted much attention, since the orbital order can be directly probed by the RXS signals on the orbital superlattice spots. Several RXS experiments have been carried out on typical perovskite compounds,^{1,2,3,4,5,6,7} in which an orbitally ordered state may be stabilized below a critical temperature.^{8,9} For the K edge in transition-metal compounds, RXS intensities arise from the modulation of $4p$ states in the intermediate states of the resonant process. Since $4p$ states are not the states of orbital ordering, this causes complications on the interpretation of RXS intensities.

A mechanism was proposed that the modulation of $4p$ states comes from orbitally polarized $3d$ states on the Mn^{3+} ion through the anisotropic terms of the $3d$ – $4p$ Coulomb interaction in LaMnO_3 ,^{10,11} and thereby it was argued that the RXS intensities on the superlattice spots are a direct reflection of orbital order. On the other hand, subsequent studies based on band structure calculations^{12,13,14} have revealed that $4p$ states of Mn^{3+} ion so extend in space that they are considerably modified by neighboring electronic states through the Jahn-Teller distortion (JTD). It has been concluded that the effect of the JTD on the RXS spectra is much larger than that of the $3d$ – $4p$ Coulomb interaction.

RXS experiments were carried out also on YVO_3 [6] and YTiO_3 [7]. Since the JTD is considerably smaller in these materials than in LaMnO_3 , one may think the effect of the Coulomb interaction important. This is not the case, though; *ab initio* calculations indicated that the effect of lattice distortion on RXS intensities is much larger than that of the $3d$ – $4p$ Coulomb interaction even in these

materials.^{15,16} The calculation was carried out within the muffin-tin (MT) approximation on the lattice parameters determined from the experiment. Since the MT approximation averages the potential coming from orbitally polarized $3d$ states, it works to eliminate the effect of the anisotropic terms of the $3d$ – $4p$ Coulomb interaction on the $4p$ states. We found that the spectra consist of several peaks, to which the GdFeO_3 -type distortion and the JTD contribute differently, in good agreement with the experiment.

Recently, an RXS experiment has been carried out on KCuF_3 , in which the intensities on the magnetic and orbital superlattice spots have been reported.^{17,18} The magnetic RXS has been studied for typical materials such as CoO [19] and NiO [20]. However, the analyses of the experimental data are limited to model calculations.^{21,22} As regards the intensities on the orbital spots, they increase with going down through the Néel temperature in the experiment, and are interpreted as a consequence of the increase of the $3d$ orbital order parameter in the magnetic phase.¹⁷ This interpretation seems obscure unless it is clarified how the $3d$ orbital order controls the RXS spectra. The purpose of this paper is to elucidate the mechanism of the RXS spectra on the orbital and magnetic superlattice spots through *ab initio* calculations. We use the full-potential linearized augmented plane wave (FLAPW) method in the LDA+ U scheme, where the local $3d$ – $3d$ Coulomb interaction is introduced on Cu sites.²³

We obtain the RXS intensity on magnetic spots by taking account of the spin-orbit interaction (SOI). The calculation has to be accurate, since the intensities are about three orders of magnitudes smaller than those on orbital spots. This seems the first case to have evalu-

ated the magnetic RXS spectra in the *ab initio* level. We reproduce well the experimental spectra as functions of photon energy and of azimuthal angle. No intensity appears without the SOI, indicating that the intensity arises from the orbital polarization, not from the spin polarization, in the $4p$ states. On the other hand, the spectra change little with turning off the SOI from the $3d$ states. Since the $3d$ orbital moment disappears in this condition, the $3d$ orbital moment plays no role to induce the orbital polarization in $4p$ states. This shows a contrast with the magnetic RXS in NiO and CoO, where the $3d$ orbital moment plays an important role through the mixing of the $4p$ states with the $3d$ states of neighboring Cu sites and the intra-atomic $4p$ - $3d$ Coulomb interaction.

We also calculate the RXS spectra on the orbital superlattice spots. A similar calculation has already been carried out.¹⁸ We come to the same conclusion that the RXS intensity is mainly controlled by lattice distortion. We add several aspects of making clear the mechanism by calculating the spectra with changing magnitude of the JTD and in various magnetic phases. We explicitly show that the magnetic order itself has little influence on the intensity and that the intensity increases with increasing JTD strength. In this respect, the increase of the intensity with passing through the Neél temperature has to accompany a considerable increase of the JTD strength in the magnetic phase. We also predict a new azimuthal angle dependence different from the previously assumed one but consistent with the experiment.¹⁸

In Sec. II, we study electronic structures in various phases with the FLAPW method in the LDA+ U scheme. In Sec. III, the absorption spectra and the RXS spectra are presented in comparison with the experiment. Section IV is devoted to concluding remarks.

II. ELECTRONIC STRUCTURES

KCuF₃ has a typical perovskite structure, and undergoes a structural phase transition at $T \approx 800$ K, below which the JTD and the associated antiferro-orbital (AFO) long-range order emerges with the ordering vector $\mathbf{Q}_{\text{orb}} = (\pi/a, \pi/b, \pi/c)$. Figure 1 shows the schematic view of the ordering pattern. It is tetragonal with $a = b = 4.141\text{\AA}$, $c = 3.924\text{\AA}$ at room temperature; three different bond lengths are given by $\ell = 2.253\text{\AA}$, $s = 1.888\text{\AA}$, $m = 1.962\text{\AA}$.^{24,25} Since the lattice parameters are not known at low temperatures, we use these values in the following calculation. There are two inequivalent Cu sites in a unit cell, which will be called as A and B sites. With further decreasing temperatures, an antiferromagnetic (AFM) long-range order develops below 38 K with the ordering vector $\mathbf{Q}_{\text{mag}} = (0, 0, \pi/c)$. Therefore four inequivalent Cu sites, A₊, A₋, B₊, B₋, exist. The local magnetic moment is pointing to either the (110) or (1 $\bar{1}$ 0) direction with the value $0.48 \mu_B$. The recent magnetic scattering experiment gives the ratio of the orbital angular momentum (L) to the spin angular

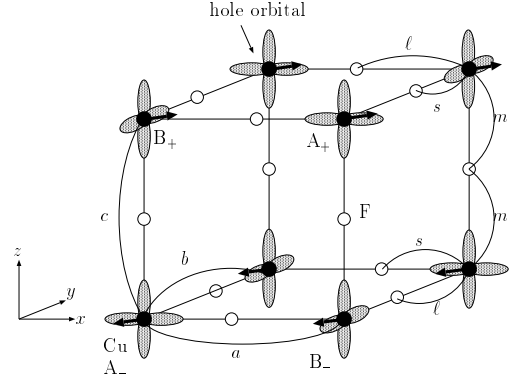


FIG. 1: Sketch of the ordering pattern of KCuF₃. Orbitals $\psi_{x^2-z^2}$ and $\psi_{y^2-z^2}$ are antiferro-orbitally ordered with the ordering vector $\mathbf{Q}_{\text{orb}} = (\pi/a, \pi/b, \pi/c)$. Arrows represent the direction of magnetic moments with the ordering vector $\mathbf{Q}_{\text{mag}} = (0, 0, \pi/c)$. Small solid spheres represent F atoms. K atoms are omitted in the figure.

momentum (S) as $L/S = 0.29$.¹⁸

We carry out the band structure calculation in the LDA+ U scheme by setting the parameters of the intraatomic Coulomb interaction between $3d$ orbitals such that $U = 3.0$ eV and $J = 1.0$ eV. We take account of the SOI to deal with the orbital moment, which is important for the RXS spectra on the magnetic spots. First assuming the AFM long-range order, we obtain an orbital long-range order with the ordering vector \mathbf{Q}_{orb} ; the hole numbers inside the Cu MT sphere in the $3d$ states $\varphi_{x^2-z^2}$ ($\varphi_{y^2-z^2}$) and $\varphi_{3y^2-r^2}$ ($\varphi_{3x^2-r^2}$) are given by $n_{x^2-z^2}(n_{y^2-z^2}) = 0.65$ $n_{3y^2-r^2}(n_{3x^2-r^2}) = 0.08$ in A_± (B_±) sites, respectively. Note that the difference in the values between A₊ and A₋ sites and B₊ and B₋ sites is negligibly small. The local magnetic moment is obtained as $0.79\mu_B$ with $S = 0.34$, $L = 0.11$, $L/S = 0.33$, which is somewhat larger than the experimental one. In order to see the effect of the magnetic order on orbital polarization, we carry out the same LDA+ U calculation in the presence of the ferromagnetic (FM) long-range order. We obtain the same type of orbital order, in which $n_{x^2-z^2}(n_{y^2-z^2}) = 0.66$ $n_{3y^2-r^2}(n_{3x^2-r^2}) = 0.10$ in A (B) sites, respectively. Since the hole numbers are similar to that of the antiferromagnetic state, we conclude that the magnetic order has little influence on the orbital order parameter. On the other hand, the orbital polarization is rather sensitive to the intraatomic Coulomb interaction. The simple LDA ($U = 0$) gives the orbital polarization much smaller than the values mentioned above, that is, $n_{x^2-z^2}(n_{y^2-z^2}) = 0.26$ and $n_{3y^2-r^2}(n_{3x^2-r^2}) = 0.11$ per spin in the A(B) sites in the nonmagnetic (NM) phase.

Figure 2 shows the calculated density of states (DOS) projected on the d and p symmetries of a Cu site, which is defined inside the MT sphere, in the AF phase given by the LDA+ U method. The origin of the energy is the bottom of the conduction band. The DOS projected onto

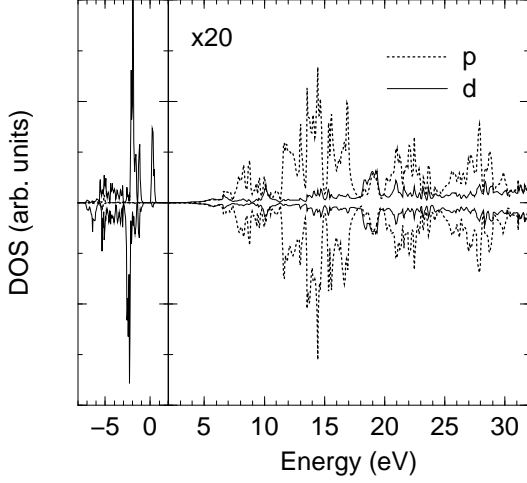


FIG. 2: Density of states projected on the s , p and d symmetric states inside the Cu muffin-tin sphere, calculated in the AFM phase of the LDA+ U scheme. The origin of energy is the bottom of the conduction band.

the d symmetric states is almost concentrated in the region of energy less than 2 eV. It has a finite gap ~ 0.82 eV. The left part of DOS is shown in a 20 times magnified scale. The most part of probability distributes in the interstitial region or on neighboring MT spheres, and thereby the magnitude of the DOS projected onto the p symmetry becomes much smaller than the $3d$ DOS. We refer to the p symmetric states as $4p$ states, because the wave functions are quite close to the atomic $4p$ wave functions within the MT sphere. Of course the “ $4p$ ” states lose the atomic character outside the MT sphere, forming an energy band with its width being as large as 30 eV. The $4p$ DOS shows almost no exchange splitting in spite of the magnetic ground state, indicating that the $3d$ states have little influence on $4p$ states.

III. ABSORPTION COEFFICIENT AND RXS SPECTRA

We define the $1s$ – $4p$ dipole transition density matrix $\tau_{mm'}^{(j)}(\varepsilon)$ assigned to each Cu site as

$$\tau_{mm'}^{(j)}(\varepsilon) = \sum_{n,\mathbf{k}} \int r^2 dr r'^2 dr' [R_{j1s}^*(r) r \mathcal{P}_m^{(j)} \phi_{n,\mathbf{k}}(r)]^* \times [R_{j1s}^*(r') r' \mathcal{P}_{m'}^{(j)} \phi_{n,\mathbf{k}}(r')] \delta(\varepsilon - \varepsilon_{n,\mathbf{k}}), \quad (3.1)$$

where j stands for sublattices A_{\pm} or B_{\pm} . Suffixes m, m' represent the x, y , and z axes, which are chosen to be parallel to the a, b , and c axes, respectively (see Fig. 1). The $\phi_{n,\mathbf{k}}$ represents the wave function with the band index n , wave-vector \mathbf{k} and energy $\varepsilon_{n,\mathbf{k}}$ which is larger than the Fermi energy. Operator $\mathcal{P}_m^{(j)}$ projects the wave function $\phi_{n,\mathbf{k}}$ on the m ($m \in x, y, z$) component of the

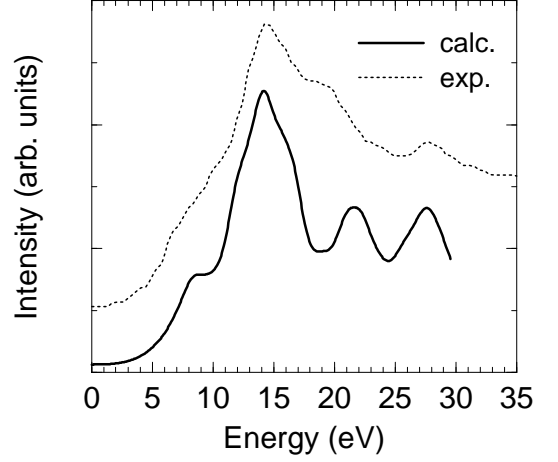


FIG. 3: Absorption coefficient $A(\omega)$ as a function of photon energy around the K edge of Cu, in comparison with the experimental data of fluorescence (Ref. 18). The core-hole energy is adjusted such that the calculated peak position coincides with the experimental one.

p symmetric part on the Cu j site. The R_{j1s} represents the Cu $1s$ wave function on the Cu j site. We evaluate this density matrix using the FLAPW wave function.

A. Absorption Coefficient

We first discuss the absorption coefficient $A(\omega)$ around the K edge. Neglecting the core-hole potential working on the $4p$ states in the final state of the absorption process, we have the expression for $A(\omega)$,

$$A(\omega) \propto \sum_{n,\mathbf{k}} \left| \int r^2 dr R_{1s}^*(r) r \mathcal{P}_m \phi_{n,\mathbf{k}}(r) \right|^2 \delta(\omega - \varepsilon_{n,\mathbf{k}} - \varepsilon_{1s}) \\ = \tau_{xx}^{(j)}(\omega - \varepsilon_{1s}) + \tau_{yy}^{(j)}(\omega - \varepsilon_{1s}) + \tau_{zz}^{(j)}(\omega - \varepsilon_{1s}), \quad (3.2)$$

where ε_{1s} is the energy of the $1s$ state. The dependence on sublattices can be neglected. $A(\omega)$ is nearly proportional to the $4p$ DOS. Figure 3 shows the calculated result in comparison with the experiment, where ε_{1s} is adjusted such that the position of the main peak coincides with the experimental one. It is difficult to determine the absolute value of ε_{1s} within the present status of the *ab initio* calculation, since several screening processes are neglected. The spectral shape is found in good agreement with the experimental curve. If the core-hole potential would be taken into account, the intensities in low frequency region may be further enhanced.

B. RXS Spectra

The conventional RXS geometry is shown in Fig. 4; photon with frequency ω , momentum \mathbf{q}_i , polarization μ

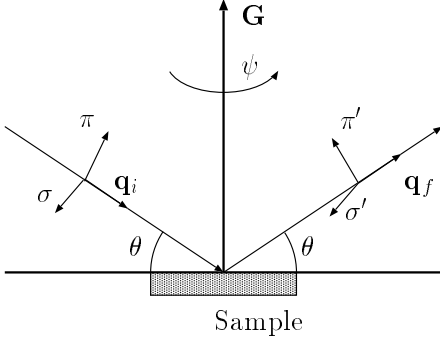


FIG. 4: RXS geometry. Incident photon with wave vector \mathbf{q}_i and polarization σ or π is scattered into the state with wave vector \mathbf{q}_f and polarization σ' or π' at Bragg angle θ . The sample crystal is rotated by azimuthal angle ψ around the scattering vector \mathbf{G} .

($= \sigma$ or π) is scattered into state with momentum \mathbf{q}_f and polarization μ' ($= \sigma'$ or π'). The scattering vector \mathbf{G} is defined by $\mathbf{q}_f - \mathbf{q}_i$. In such a situation, we have the RXS intensity $I(\mathbf{G}, \omega)$

$$I(\mathbf{G}, \omega) \propto \left| \sum_{mm'} E_m^{\text{out}} M_{mm'}(\mathbf{G}, \omega) E_m^{\text{in}} \right|^2, \quad (3.3)$$

with

$$M_{mm'}(\mathbf{G}, \omega) = \frac{1}{\sqrt{N}} \sum_{j, \Lambda} \frac{\langle g | x_m(j) | \Lambda \rangle \langle \Lambda | x_{m'}(j) | g \rangle}{\hbar\omega - (E_\Lambda - E_g) + i\Gamma} \exp(-i\mathbf{G} \cdot \mathbf{r}_j). \quad (3.4)$$

Here $E_x^{\text{in(out)}}$ is the x component of polarization vector of the incident (scattered) photon, and j runs over Cu lattice sites. The $|g\rangle$ represents the ground state with energy E_g . The $|\Lambda\rangle$ represents the intermediate state with energy E_Λ ; it consists of the excited electron on the $4p$ states and a hole on the $1s$ state. Γ describes the broadening due to the $1s$ core-hole lifetime. The RXS spectra are rather insensitive with varying Γ values; we set $\Gamma = 1$ eV. The dipole operators $x_\alpha(j)$ at site j are defined as $x_1(j) = x$, $x_2(j) = y$, $x_3(j) = z$ in the coordinate frame fixed to the crystal axes with the origin located at the center of site j . Hereafter \mathbf{G} is expressed in unit of $(2\pi/2a, 2\pi/2b, 2\pi/2c)$. Just like the absorption coefficient, we neglect the core-hole potential in the intermediate state. Then the amplitude $M_{mm'}(\mathbf{G}, \omega)$ is expressed in terms of the density matrices:

$$M_{mm'}(\mathbf{G}, \omega) = \frac{1}{\sqrt{N}} \sum_j \exp(-i\mathbf{G} \cdot \mathbf{r}_j) \int \frac{\tau_{mm'}^{(j)}(\varepsilon) d\varepsilon}{\hbar\omega - \varepsilon + \varepsilon_{1s} + i\Gamma}. \quad (3.5)$$

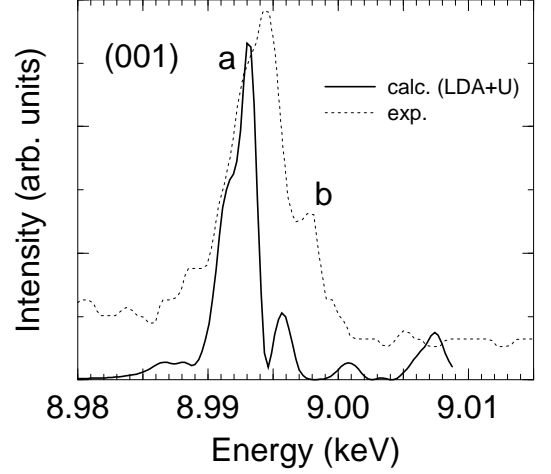


FIG. 5: Calculated RXS spectra on a magnetic superlattice spot (001) in comparison with the experiment (Ref. 18). The core-hole energy is set the same as in the case of absorption coefficient (Fig. 3).

1. on Magnetic Superlattice Spots

For the magnetic superlattice spots $\mathbf{G} = (00m)$ with m being odd integers, Eq.(3.5) contains the following combination of density matrices:

$$\begin{aligned} & \tau^{(A+)}(\varepsilon) - \tau^{(A-)}(\varepsilon) + \tau^{(B+)}(\varepsilon) - \tau^{(B-)}(\varepsilon) \\ &= \begin{pmatrix} 0 & 0 & \eta(\varepsilon) \\ 0 & 0 & \eta(\varepsilon) \\ -\eta(\varepsilon) & -\eta(\varepsilon) & 0 \end{pmatrix}. \end{aligned} \quad (3.6)$$

Only the off-diagonal elements survives with an antisymmetric form.^{21,22} They would vanish without the SOI, indicating that they arise from the *orbital polarization*³² in the $4p$ states. From this expression, Eq.(3.5) becomes

$$I(\mathbf{G}, \omega) \propto \left| (C_{yz} + C_{zx}) \int d\varepsilon \frac{\eta(\varepsilon)}{\omega - \varepsilon + \varepsilon_{1s} + i\Gamma} \right|^2, \quad (3.7)$$

with $C_{ij} = E_i^{\text{out}} E_j^{\text{in}} - E_j^{\text{out}} E_i^{\text{in}}$. Since the polarization dependent part $C_{yz} + C_{zx}$ is factored out, the photon energy dependence is independent of polarization.

The actual calculation in the LDA+ U scheme is rather heavy, since the number of atoms in the unit cell becomes as large as 20 in the AFM phase. Highly accurate calculations are required, since the intensity is about three orders of magnitude smaller than that for the orbital superlattice spots, as shown below. It is not easy to sum up many \mathbf{k} -points in evaluating $\eta(\varepsilon)$, though. Fortunately, summing $8 \times 8 \times 8$ \mathbf{k} -points in the first Brillouin zone seems sufficient in comparison with the result for summing $6 \times 6 \times 6$ \mathbf{k} -points. Figure 5 shows the calculated spectra for $\mathbf{G} = (001)$ as a function of photon energy in comparison with the experiment.¹⁸ The intensity in the the $\sigma \rightarrow \sigma'$ channel does not appear in agreement with

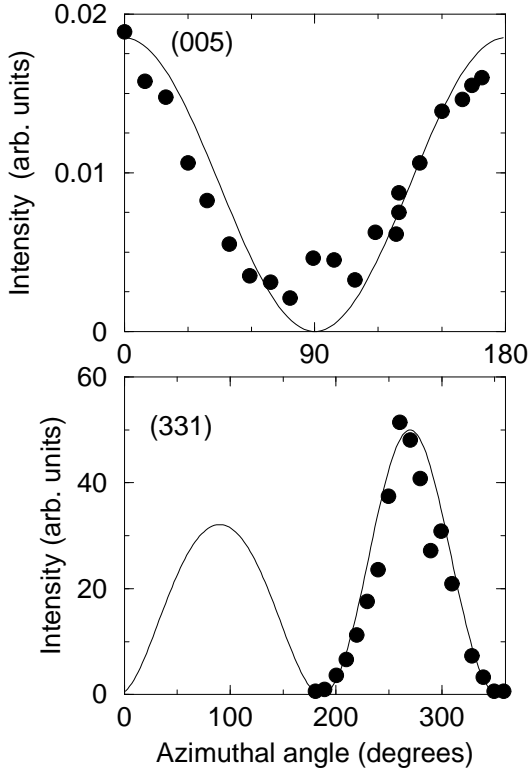


FIG. 6: Azimuthal angle dependence of the peak intensity on a magnetic superlattice spot (005) and on an orbital superlattice spot (331), in comparison with the experiment (Ref. 18).

the experiment. Its spectral shape consists of several peaks. The highest and next highest peaks correspond well to peaks a and b, although their energies are slightly shifted. Note that the core-hole energy has already been adjusted such that the calculated absorption peak coincides with the experimental one. We have checked that the spectra change little with turning off the SOI from the $3d$ states. This suggests that the $3d$ orbital moment has little influence on inducing the $4p$ orbital polarization.

From Eq. (3.7), we derive explicitly the azimuthal angle dependence,

$$I(\mathbf{G}, \omega) \propto 0 \quad \text{for } \sigma \rightarrow \sigma' \\ \propto |\cos \theta \cos \psi|^2 \quad \text{for } \sigma \rightarrow \pi', \quad (3.8)$$

where $\sin \theta = 0.088$ for the (001) spot and $\sin \theta = 0.439$ for the (005) spot. Here the azimuthal angle $\psi = 0$ is defined such that the $(\bar{1}10)$ axis is contained in the scattering plane. Figure 6 shows the peak intensity on (005) as a function of ψ , in comparison with the experiment. The dependence agrees with the experiment.

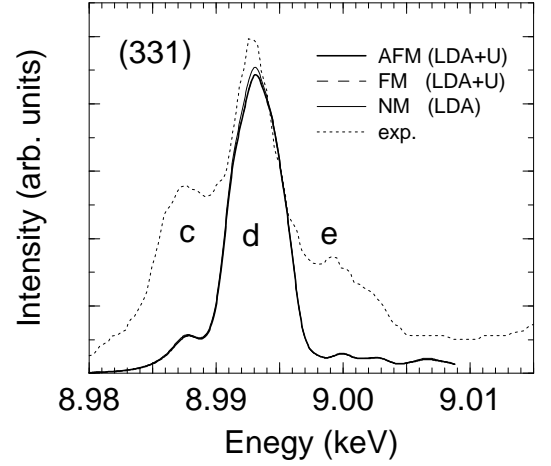


FIG. 7: Calculated RXS spectra on an orbital superlattice spot (331) in comparison with the experiment. The thick solid and broken lines show the spectra on the AFM and FM phases in the LDA+ U scheme, respectively. The thin solid line shows the spectra on the NM phase in the LDA scheme. The dotted line shows the experimental data (Ref.[18]). The core-hole energy is set the same as in the case of absorption coefficient.

2. on Orbital Superlattice Spots

For the orbital superlattice spots $\mathbf{G} = (hlm)$ with h, l , and m being odd integers, Eq. (3.5) contains the following combination of density matrices:

$$\tau^{(A+)}(\varepsilon) + \tau^{(A-)}(\varepsilon) - \tau^{(B+)}(\varepsilon) - \tau^{(B-)}(\varepsilon) \\ \approx \begin{pmatrix} \alpha(\varepsilon) - \beta(\varepsilon) & 0 & \gamma(\varepsilon) \\ 0 & \beta(\varepsilon) - \alpha(\varepsilon) & \delta(\varepsilon) \\ -\gamma(\varepsilon) & -\delta(\varepsilon) & 0 \end{pmatrix}. \quad (3.9)$$

The off-diagonal elements are about two orders of magnitude smaller than the diagonal terms. Neglecting such terms, we obtain

$$I(\mathbf{G}, \omega) \propto \left| C_{x^2-y^2} \int d\varepsilon \frac{\alpha(\varepsilon) - \beta(\varepsilon)}{\omega - \varepsilon + \varepsilon_{1s} + i\Gamma} \right|^2, \quad (3.10)$$

with

$$C_{x^2-y^2} = E_x^{\text{out}} E_x^{\text{in}} - E_y^{\text{out}} E_y^{\text{in}}. \quad (3.11)$$

Just like Eq. (3.7), the polarization dependent part $C_{x^2-y^2}$ is factored out, so that the photon energy dependence becomes independent of polarization.

Figure 7 shows the calculated spectrum for $\mathbf{G} = (331)$, as a function of photon energy, in comparison with the experiment. The calculation is carried out on both the AFM and FM phases in the LDA+ U scheme, and on the NM phase in the simple LDA scheme. All three cases of calculation give nearly the same result, indicating that the $4p$ states are little influenced by the details of the $3d$ states, in agreement of the previous calculation of the

same kind.¹⁸ In particular, the fact that the last case gives the similar result in spite of considerably smaller orbital polarizations gives a strong support to the mechanism that the 3d orbital polarization has little relation to the RXS intensity. This is consistent with previous studies on other transition-metal compounds,^{12,13,14} where the RXS intensity are mainly controlled by lattice distortion. The effect of the SOI is negligibly small for the these cases. The present calculation reproduce well the spectra consisting of three peaks, although peaks c and e are much smaller than the experimental ones.

The azimuthal angle dependence for $\mathbf{G} = (331)$ is explicitly evaluated from Eq.(3.11). It is given by

$$\begin{aligned} I(\mathbf{G}, \omega) &\propto |\cos \beta \sin 2\psi|^2 \quad \text{for } \sigma \rightarrow \sigma' \\ &\propto |\sin \theta \cos \beta \cos 2\psi + \cos \theta \sin \beta \sin \psi|^2 \\ &\quad \text{for } \sigma \rightarrow \pi', \end{aligned} \quad (3.12)$$

with $\sin \theta = 0.364$, $\tan \beta = 3\sqrt{2}c/a = 4.02$. The azimuthal angle $\psi = 0$ is again defined such that the $(\bar{1}10)$ axis is contained in the scattering plane. The intensity has a period of 2π not π with respect to ψ . This rather complex behavior seems reasonable, since the scattering vector \mathbf{G} is not in a direction of high symmetry. This is obviously different from the form previously assumed in the analysis of the experimental data.¹⁸ Figure 6 shows the peak intensity as a function of ψ , in comparison with the experiment. The present form is consistent with the experiment.

So far, all the spectra are calculated with the lattice parameters at room temperature mentioned before. If the RXS intensity arises from lattice distortion, it increases with increasing JTD strength. To confirm this, we calculate the intensity with changing the JTD strength. Figure 8 shows the intensity of the peak at $\hbar\omega = 8995$ eV as a function of $\ell - s$ (the values of m and $\ell + s$ are kept to be 1.962Å and 4.141Å, respectively). The intensity monotonically increases with increasing values of $\ell - s$, consistent with the above observation. It has been observed in the experiment that the intensity increases by factor 2 with temperature going through the magnetic phase transition temperature, and this behavior has been interpreted as a consequence of a strong coupling between orbital and spin degrees of freedom.¹⁷ The result that the spectra are mainly controlled by lattice distortion indicates that the lattice distortion becomes large in the magnetic phase. The direct determination of lattice parameters have not been carried out yet.

IV. CONCLUDING REMARKS

We have calculated the RXS spectra around the K edge of Cu in KCuF_3 on the basis of the *ab initio* calculation, that is, the FLAPW method in the LDA+ U scheme. The lattice distortion is introduced as inputs of calculation. We have obtained finite intensities on magnetic superlattice spots by taking account of the SOI. The

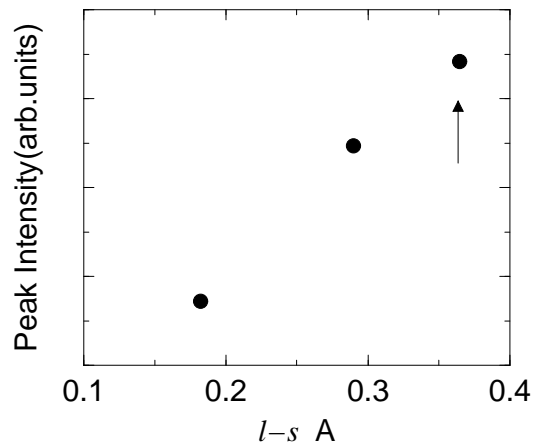


FIG. 8: Peak intensity of RXS spectra on (331) with varying JTD strength. The values of m and $\ell + s$ are fixed at 1.962Å and 4.141Å, respectively. The circle indicated by an arrow is the result for the actual value of $\ell - s$ at room temperature.

intensities are about three orders of magnitude smaller than those on orbital superlattice spots, consistent with the experiment. This is the first result to have evaluated the magnetic RXS spectra in the *ab initio* level. Since the intensity disappears without the SOI, the present result indicates that the spectra arises from the orbital polarization, not from the spin polarization, in the 4p states. On the other hand, the spectra change little with turning off the SOI from the 3d states. This indicates that the 3d orbital moment has no role to induce the 4p orbital polarization. This situation is different from our previous finding in the study of the magnetic RXS in CoO and NiO that the 4p orbital polarization is induced by the 3d orbital moment through the mixing of the 4p states with the 3d states of *neighboring* Cu atoms and the intra-atomic 4p-3d Coulomb interaction.^{21,22} This difference may come from the fact that the 3d orbital moment is about 1/3 of that in NiO and 1/10 of that in CoO. Furthermore, the mixing effect may become smaller than in NiO and CoO, since neighboring Cu sites are always intervened by F atoms. Closely related is the phenomenon of the magnetic circular dichroism (MCD) in the K -edge absorption in ferromagnetic metals Fe, Co, Ni.²⁶ In this case, the 4p orbital polarization was found to be induced by the 3d orbital moment through the 4p mixing with the 3d states at *neighboring* sites.^{27,28}

We have also calculated the RXS intensities on orbital superlattice spots. The spectra are independent of whether the system is in the AFM phase or in the FM phase, and of the orbital polarization in the 3d states. We have explicitly shown that the spectra are mainly controlled by the lattice distortion through the calculation with varying JTD strength. The present result is consistent with the previous studies of the RXS on transition-metal oxides,^{12,13,14,15,16} but shows contrast with the RXS around the L_{III} edge in the quadrupole

ordering phase of the rare-earth compound CeB_6 , where the spectra seems directly controlled by the quadrupole order.^{29,30,31}

Acknowledgments

We have used the FLAPW code developed by N. Hamada. We thank him for allowing to use his code.

This work was partially supported by a Grant-in-Aid for Scientific Research from the Ministry of Education, Culture, Sports, Science, and Technology, Japan.

-
- ¹ Y. Murakami, H. Kawata, M. Tanaka, T. Arima, Y. Moritomo, and Y. Tokura, *Phys. Rev. Lett.* **80**, 1932 (1998).
 - ² Y. Murakami, J. P. Hill, D. Gibbs, M. Blume, I. Koyama, M. Tanaka, H. Kawata, T. Arima, Y. Tokura, K. Hirota, et al., *Phys. Rev. Lett.* **81**, 582 (1998).
 - ³ Y. Endoh, K. Hirota, S. Ishihara, S. Okamoto, Y. Murakami, A. Nishizawa, T. Fukuda, H. Kimura, H. Nojiri, K. Kaneko, et al., *Phys. Rev. Lett.* **82**, 4328 (1999).
 - ⁴ K. Nakamura, T. Arima, A. Nakazawa, Y. Wakabayashi, and Y. Murakami, *Phys. Rev. B* **60**, 2425 (1999).
 - ⁵ M. von Zimmermann, J. Hill, D. Gibbs, M. Blume, D. Casa, B. Keimer, Y. Murakami, Y. Tomioka, and Y. Tokura, *Phys. Rev. Lett.* **83**, 4872 (1999).
 - ⁶ M. Noguchi, A. Nakazawa, T. Arima, Y. Wakabayashi, H. Nakao, and Y. Murakami, *Phys. Rev. B* **62**, R9271 (2000).
 - ⁷ H. Nakao, Y. Wakabayashi, T. Kiyama, and Y. Murakami (unpublished).
 - ⁸ J. Kanamori, *J. Appl. Phys.* **31**, 14S (1960).
 - ⁹ K. I. Kugel and D. I. Khomskii, *JETP Lett.* **15**, 446 (1972).
 - ¹⁰ S. Ishihara and S. Maekawa, *Phys. Rev. Lett.* **80**, 3799 (1998).
 - ¹¹ S. Ishihara and S. Maekawa, *Phys. Rev. B* **58**, 13449 (1998).
 - ¹² I. S. Elfimov, V. I. Anisimov, and G. Sawatzky, *Phys. Rev. Lett.* **82**, 4264 (1999).
 - ¹³ M. Benfatto, Y. Joly, and C. R. Natoli, *Phys. Rev. Lett.* **83**, 636 (1999).
 - ¹⁴ M. Takahashi, J. Igarashi, and P. Fulde, *J. Phys. Soc. Jpn.* **68**, 2530 (1999).
 - ¹⁵ M. Takahashi and J. Igarashi, *Phys. Rev. B* **64**, 075110 (2001).
 - ¹⁶ M. Takahashi and J. Igarashi, *Phys. Rev. B* **65**, 205114 (2002).
 - ¹⁷ L. Paolasini, R. Caciuffo, A. Sollier, P. Ghigna, and M. Altarelli, *Phys. Rev. Lett.* **88**, 106403 (2002).
 - ¹⁸ R. Caciuffo, L. Paolasini, A. Sollier, P. Ghigna, E. Pavarini, J. van den Brink, and M. Altarelli, *Phys. Rev. B* **65**, 174425 (2002).
 - ¹⁹ W. Neubeck, C. Vettier, K.-B. Lee, , and F. de Bergevin, *Phys. Rev. B* **60**, R9912 (1999).
 - ²⁰ W. Neubeck, C. Vettier, F. de Bergevin, F. Yakhov, D. Mannix, O. Bengone, M. Alouani, and A. Barbier, *Phys. Rev. B* **63**, 134430 (2001).
 - ²¹ J. Igarashi and M. Takahashi, *J. Phys. Soc. Jpn.* **69**, 4087 (2000).
 - ²² J. Igarashi and M. Takahashi, *Phys. Rev. B* **63**, 184430 (2001).
 - ²³ V. I. Anisimov, F. Aryasetiawan, , and A. I. Lichtenstein, *J. Phys. Condens. Matter* **9**, 767 (1997).
 - ²⁴ R. H. Buttner, E. N. Maslen, and N. Spadaccini, *Acta Cryst.* **B46**, 131 (1990).
 - ²⁵ M. T. Hutchings, E. J. Samuelsen, G. Shirane, and K. Hirakawa, *Phys. Rev.* **188**, 919 (1969).
 - ²⁶ G. Schütz, W. Wagner, W. Wilhelm, P. Kienle, R. Zeller, R. Frahn, and G. Materlik, *Phys. Rev. Lett.* **58**, 737 (1987).
 - ²⁷ J. Igarashi and K. Hirai, *Phys. Rev. B* **50**, 17820 (1994).
 - ²⁸ J. Igarashi and K. Hirai, *Phys. Rev. B* **53**, 6442 (1996).
 - ²⁹ H. Nakao, K. Magishi, Y. Wakabayashi, Y. Murakami, K. Koyama, K. Hirota, Y. Endoh, and S. Kunii, *J. Phys. Soc. Jpn.* **70**, 1857 (2001).
 - ³⁰ T. Nagao and J. Igarashi, *J. Phys. Soc. Jpn.* **70**, 2892 (2001).
 - ³¹ J. Igarashi and T. Nagao, *J. Phys. Soc. Jpn.* **71**, 1771 (2002).
 - ³² The orbital polarization in the $4p$ states here means the polarization related to imaginary wavefunctions, which gives rise to orbital moment. On the other hand, the $4p$ orbital polarization for the case of orbital superlattice spots means the polarization with respect to real wavefunctions such as x , y , z types.